

# Active control of supersonic impingement tones using steady and pulsed microjets

Jae Jeen Choi · Anuradha M. Annaswamy ·  
Huadong Lou · Farrukh S. Alvi

Received: 3 June 2005 / Revised: 10 July 2006 / Accepted: 11 July 2006 / Published online: 10 October 2006  
© Springer-Verlag 2006

**Abstract** In recent years, it has been demonstrated that direct microjet injection into the shear layer of the main jet disrupts the feedback loop inherent in high speed impinging jet flows, thereby significantly reducing the adverse effects. The amount of noise reduced by microjet actuation is known to be dependent on nozzle operating conditions. In this paper, two active control strategies using microjets are suggested to maintain a uniform, reliable, and optimal reduction of these tones over the entire range of operating conditions. In the first method, a quasi-closed loop control strategy is proposed using steady microjet injection and the proper orthogonal decomposition (POD) algorithm. The most energetic spatial mode of the unsteady pressure along the nozzle diameter is captured using the POD, which in turn is used to determine the distribution of microjet intensity along the nozzle exit. Preliminary experimental results from a STOVL supersonic jet facility at Mach 1.5 show that the quasi-closed loop control strategy, in some cases, provides an additional 8–10 dB reduction compared to axisymmetric injection at the desired operating conditions.

The second method consists of a pulsed microjet injection, motivated by the need to further improve the noise suppression. It was observed that the pulsed microjet was able to bring about the same noise reduction as steady injection using approximately 40% of the corresponding mass flow rate of the steady microjet case. Moreover, as the duty cycle increased, the performance of pulsed injection was further enhanced and was observed to completely eliminate the impinging tones at all operating conditions.

## 1 Introduction

While hovering in close proximity to the ground, the short take off and vertical landing (STOVL) aircraft experiences discrete and high amplitude acoustic tones that are produced via a feedback process. These feedback interactions occur thus: instability waves are generated by the acoustic excitation of the shear layer near the nozzle exit, which then convect down and evolve into spatially coherent structures. Upon impinging on the ground, these structures generate acoustic waves, which in turn excite the shear layer at the nozzle exit, thereby closing the feedback loop (Fig. 1; Krothapalli et al. 1999; Alvi et al. 2003). The high amplitude impingement tones are undesirable not only due to the associated high ambient noise, but also due to the accompanied unsteady pressure loads on the ground plane and the nearby surfaces. While the high noise levels can lead to structural fatigue of the aircraft surfaces in the vicinity of the nozzles, the dynamic loads on the impingement surface can lead to an

---

J. J. Choi (✉) · A. M. Annaswamy  
Department of Mechanical Engineering,  
Massachusetts Institute of Technology,  
Room 3-441, 77 Massachusetts Ave,  
Cambridge, MA 02139-4307, USA  
e-mail: jaejeen@mit.edu

H. Lou · F. S. Alvi  
Department of Mechanical Engineering, FAMU - FSU,  
College of Engineering, 2525 Pottsdamer Street Rm229,  
Tallahassee, FL 32310, USA  
e-mail: alvi@eng.fsu.edu

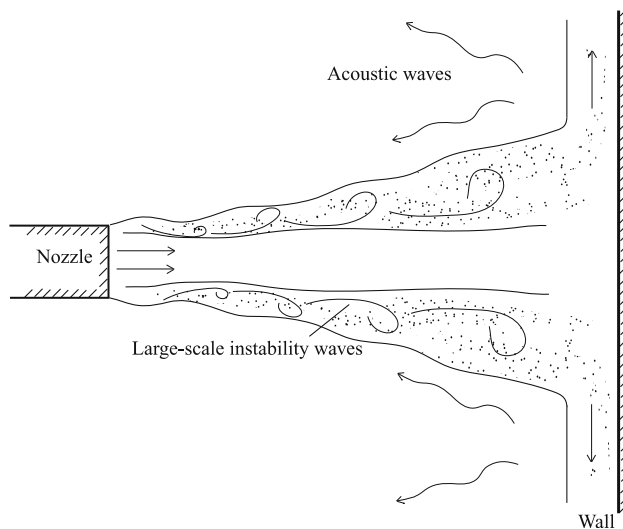


**Fig. 1** Schematic diagram of an impinging jet and possible feedback path

increased erosion of the landing surface as well as a dramatic lift loss during hover.

In an effort to reduce or eliminate these tones, several passive (Glass 1968; Poldervaart et al. 1974; Elavarasan et al. 2002) and active control methods (Sheplak and Spina 1994; Shih et al. 1999; Alvi et al. 2003) have been attempted over the years to modify the feedback loop. Of these, the technique in Alvi et al. (2003) appears most promising from the point of view of efficiency, flexibility, and robustness. The method in Alvi et al. (2003) introduces microjets along the periphery of the nozzle exit which modify the shear layer at its most receptive location thereby efficiently attenuating the impingement tones. Due to their small size, these microjets can be optimally distributed along the circumference and can also be introduced on-demand.

In Alvi et al. (2003), the microjets were injected with a steady-flow along the nozzle periphery, with the value maintained at a constant, independent of the impinging flow-field. This open-loop control strategy led, at certain heights, to the distinct tones either getting diminished or completely removed. There was an overall decline in the unsteadiness of the flow as well. Figure 2 shows the OASPL plot for different height conditions obtained using a 20° microjet injection with respect to the nozzle axis. It is also observed in Fig. 2 that the magnitude of suppression is dependent to a large extent on the operating conditions and that the magnitude of reduction varies with the height of the lift plate from the ground as well as with the flow conditions. Since in practice, the operating conditions are expected to change significantly during take-off

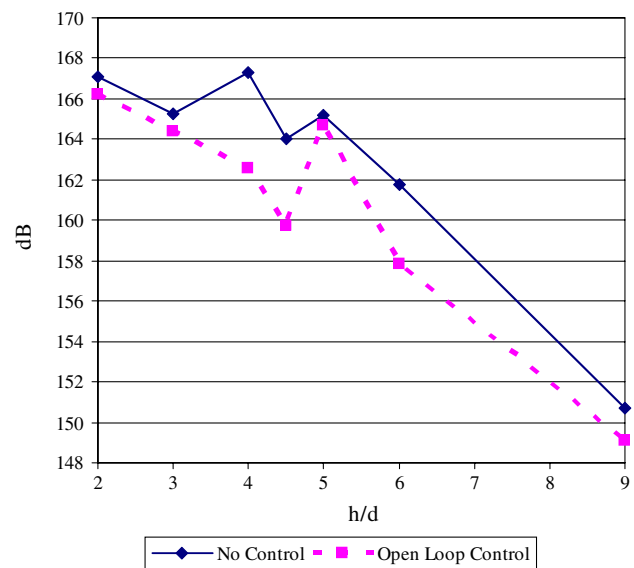


**Fig. 2** Overall sound pressure level measurement, 115 psia supply pressure and 20° microjet injection angle

and landing, a more attractive control strategy is ‘closed-loop control,’ where the microjet effect is modified using suitable measurement of the impinging flow field, thereby maintaining a uniform noise reduction over a large range of operating conditions. In fact, it is well-known that for flows governed by a feedback loop, such as the present flow, screeching jets, and others, the flowfield properties can change measurably even when the nominal operating conditions are the same. This is due the inherently high sensitivity of the feedback loop to very small changes in inlet and boundary conditions which can lead to changes in aeroacoustic properties (e.g., tonal frequencies and their magnitudes, Lou et al. 2002). This further emphasizes the need for an adaptive control approach for such flows. In this paper, we explore such a closed-loop control strategy for reducing the impingement tones.

A traditional approach for designing a closed-loop controller is to begin with a model that describes the impinging flow-field, and carry out a model-based control design. There are, however, two difficulties in employing such an approach for the current problem. One is that the changing boundary conditions, compressibility effects, and the feedback interactions between acoustics and the shear make the modeling significantly more complicated. The other is that the traditional feedback control paradigm typically requires the control input to be modulated at the natural frequencies of the system and mandate that the external actuator have the necessary bandwidth for operating at the natural frequencies (Annaswamy et al.

2000). In the problem under consideration, the impinging tones associated with the flow field are typically a few kilohertz. Given the current technology, modulating the microjets at the system frequencies while producing a microjets with significant momentum is extremely difficult, if not impossible. We note that, as discussed in Cattafesta et al. (2003), the development of high-frequency and high output actuators that can operate over a large range of frequencies is much needed. Although this is an active area of research, at present such actuators are not yet available in an usable platform.

To overcome these hurdles, two different control strategies were suggested in this paper. The first approach presented modulates the control input,  $p_{\mu}$ , at a slow time-scale, so that it behaves like a parameter. Here, the control input, the azimuthal distribution of microjet pressure, is chosen from ‘proper orthogonal decomposition (POD),’ which calculates the most energetic spatial mode from given experimental data. If this control input is chosen judiciously, then even small and slow changes in this ‘parameter’ can lead to large changes in the process dynamics.

The POD method is a tool used to extract the most energetic modes from a set of realizations from an underlying system (Holmes et al. 1996). These modes can be used as basis functions for Galerkin projections of the model in order to reduce the solution space being considered to the smallest linear subspace that is sufficient to describe the system. The decomposition is ‘optimal’ in that the energy contained in an  $N$ th-ordered POD base is greater than any other  $N$ -ordered base in a mean-squared sense. Over the years, it has been applied in several disciplines including turbulence, stochastic processes, image processing, signal analysis, data compression, process identification and control in chemical engineering, and oceanography, and has been referred to by various names including Karhunen–Loeve decomposition, principal component analysis, and singular value decomposition. In fluid mechanical systems, the POD technique has been applied in the analysis of coherent structures in turbulent flows and in obtaining reduced order models to describe the dominant characteristics of the phenomena. One of the earliest studies was conducted by Bakewell and Lumley (1967) on a fully developed pipe flow. Since then, POD models have been used to model the one-dimensional Ginzburg–Landau equation (Sirovich and Rodriguez 1987), the laminar–turbulent transitional flow in a flat plate boundary layer (Rempfe 1994), pressure fluctuations surrounding a turbulent jet (Arndt et al. 1997), turbulent plane mixing layer (Delville et al. 1999), velocity field for an axisymmetric

jet (Citriniti and George 2000), low-dimensionality of a turbulent flow near wake (Ma et al. 2000), low-dimensional leading-edge vortices in the unsteady flow past a delta wing (Cipolla et al. 1998), and flow over a rectangular cavity (Rowley et al. 2000). The Eigen functions were developed using both experimental and numerical database. In this paper, we use the POD method to extract information about the mode shapes from pressure measurements which, in return, is used for control input strategy.

In the second control method, a pulsed microjet is introduced as an actuator. The rationale for doing this is that for a given mass flow rate, pulsed injection can generate larger momentum than steady continuous microjet injection, which is consequently expected to have a stronger impact on the noise reduction mechanism.

Pulsing of jet flows has been attempted in Wiltse and Glezer (1998), Sinha et al. (2002), Stanek et al. (2002a, b) and Kastner and Samimy (2003). Wiltse and Glezer (1998) introduced an open-loop control strategy via high frequency forcing in the inertial subrange of a free shear layer on a low speed flow. They found that broadband velocity fluctuations were reduced at low frequency but increased at high frequencies. Sinha et al. (2002) and Stanek et al. (2002a, b) adopted the high frequency forcing technology for control of the cavity flows and Raman and Kibens (2001) reported results applied for control of impinging tones. More recently, Kastner and Samimy (2003) reported reducing a resonant peak using Hartmann tube fluidic actuator (HTFA), a very high speed actuator for controlling the impinging jet noise. This actuator primarily worked in a blowing-mode, required a fairly large mass-flow rates, and worked over a fairly narrow range of frequencies whose selection required considerable tuning. Here, we pursue a low speed pulsing strategy which is far below the natural frequency ( $\sim 5$  kHz) of the system. The actuator used modulates the flow at the exit of the microjet using a rotating cap. Saw-tooth structures placed in the inner race of the rotating cap block and unblock the microjet holes as the cap rotates and simulates an on–off micorjet action. A similar pulsing actuator design was used to control a free jet in Ibrahim et al. (2002). However, as demonstrated in Sect. 1, the design proposed here is significantly more efficient due to the location of the actuator.

The paper begins with an explanation of the experimental setup in Sect. 2, followed by the POD-based control strategy in Sect. 3. Experimental results using this strategy are presented and compared with an open-loop control strategy. In order to improve the microjet performance further, a pulsed microjet

actuation is proposed, the details of which are presented in Sect. 4. The result of both synchronous pulsing and pulsing with a phase difference are presented and discussed.

## 2 Experimental setup

### 2.1 Test configuration and facility

The following experiments were carried out at the supersonic STOVL jet facility of the Fluid Mechanics Research Laboratory located at the Florida State University. A schematic of experimental setup with a single impinging jet is shown in Fig. 3. This facility is used primarily to study jet induced phenomenon on STOVL aircraft hovering in and out of the ground effect (Krothapalli et al. 1999; Alvi et al. 2003). A circular plate of diameter  $D$  (25.4 cm  $\sim 10d$ ) was flush mounted with the nozzle exit and, henceforth referred to as the ‘lift plate’, represents a aircraft platform. A 1 m  $\times$  1 m  $\times$  25 mm aluminum plate is mounted under the nozzle, which serves as the ground plane simulating the hovering situation by fixed it to the desired position. Further facility details can be found in Krothapalli et al. (1999).

The supersonic impinging jet was produced by an axisymmetric, convergent–divergent (C–D) nozzle with a design Mach number of 1.5. The throat and exit diameters ( $d$ ,  $d_e$ ) of the nozzle are 2.54 and 2.75 cm (Figs. 3, 4). The divergent part of the nozzle is a straight-walled conic section with a 3° divergence angle from the throat to the nozzle exit. A Validyne pressure transducer measures the stagnation pressure in the settling chamber just upstream of the nozzle. Although tests were conducted over a range of nozzle pressure ratios (NPR, where NPR = stagnation pressure/ambient pressure), the results discussed in the present paper are limited to NPR = 3.7 that corresponds to an ideally expanded Mach 1.5 jet. The nozzle total pressure was maintained within  $\pm 0.2$  psi of the desired conditions.

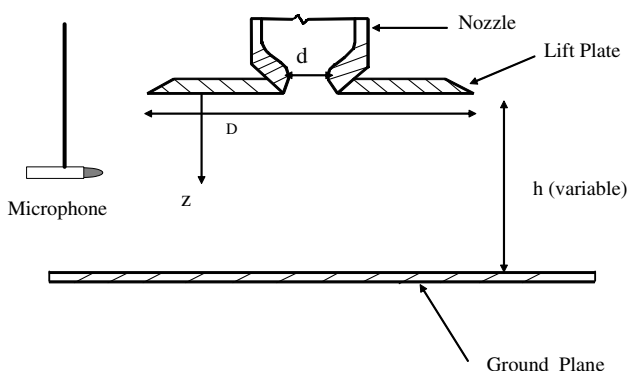


**Fig. 3** Test geometry

Sixteen microjets fabricated using 400  $\mu$ m diameter stainless tubes were used as actuators for active flow control. These are flush mounted circumferentially around the main jet as shown in Fig. 4a. While the orientation of the jets can be varied between 0° and 90°, most of the experiments reported in this paper correspond to the microjets at either 20° or 30° with respect to the nozzle axis. The supply for the microjets was provided by compressed nitrogen cylinders through a main and four secondary plenum chambers. In this manner, the supply pressures to each bank of microjets could be independently controlled. The microjets were operated over a range of NPR = 5–7, where the combined mass flow rate from all the microjets was less than 0.5% of the primary jet mass flux.

### 2.2 Pressure measurements

Near-field noise was measured using B&K™ microphones placed approximately 25 cm away from the jet.

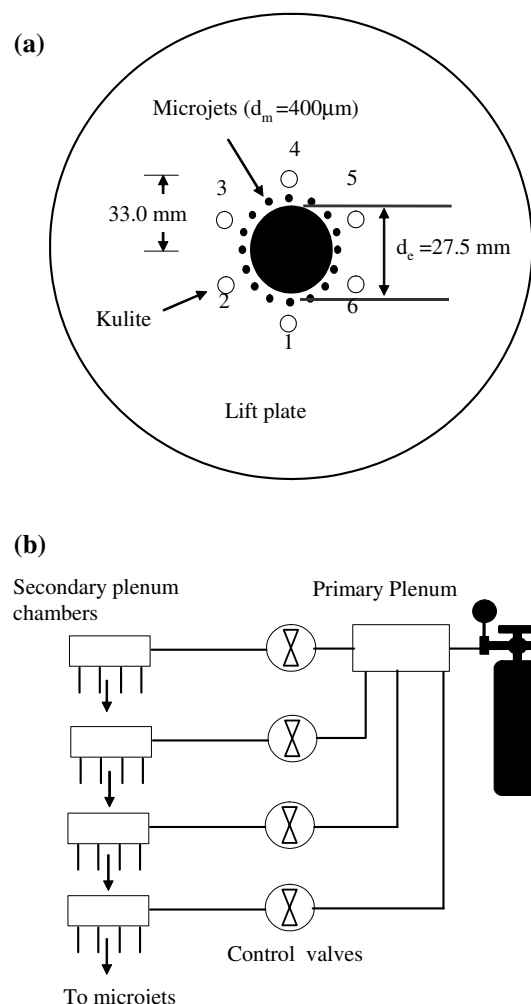


**Fig. 4** **a** Lift plate/microjet layout and **b** microjet feed assembly

The microphone signal was measured with an estimated uncertainty of  $\pm 1$  dB. The distribution of unsteady loads on the lift plate was measured by six high frequency response miniature Kulite™ pressure transducers (model: XCS-062), placed axisymmetrically around the nozzle periphery plate, at  $r/d = 1.3$  from the nozzle centerline (Fig. 4). The Kulites were frequently calibrated throughout the experiments (almost every day) where the sensitivity was found to be very close to the values quoted by the vendor, between 24 and 26 mV/psi. The use of such transducers for measuring dynamic pressures is a standard, well-established practice for low speed and high speed flows for more than a decade (Erengil and Dolling 1993; Unalmis et al. 2001; Ukeiley and Murray 2005). According to the manufacturer's specifications, these transducers have a flat frequency response up to 20% of their natural frequency. The transducers have a combined non-linearity and hysteresis (max) of  $\pm 0.5\%$ . The noise floor for these transducers was about 60 dB below the measured dynamic pressures, i.e., the signal to noise ratio was roughly 1,000. Note that lift plate *Kulites* were only used for the steady microjet experiments. They were not used for the pulsed jet studies due to the vibration of the lift plate as a result of the pulsing hardware.

The transducer output was measured using National Instruments digital data acquisition cards (PC-MIO-16E-1 card coupled with SC 2040 Sample and Hold card) and *LabView*™ software at a sampling rate of 70 kHz. The signal was low-pass filtered at 33 kHz, using Stanford Research Systems, SR640(8 pole-elliptic) Low Pass filters. These filters are phase-matched to better than  $\pm 0.75^\circ$  between channels. The phase lags between the various channels was checked by processing the known signals through the entire chain of data acquisition and conditioning hardware, e.g., filters, amplifiers, and data acquisition cards. This was done using test signals over the range of frequencies of interest in the present study. The phases between the various channels matched within  $\pm 5^\circ$ . Similar Kulite transducers have also been calibrated by Ukeiley (private communication, 2006), where the phase between different transducers was found to be within  $2^\circ$ . The results discussed in Sect. 3.3 indicate a phase difference of about  $15^\circ$ , which is well above the random error in phase introduced due to the hardware. About 100k points were recorded for each signal. Standard statistical analysis techniques were used to obtain the spectral content and the overall sound pressure level (OASPL) from these measurements. For the spectral analysis, the fast Fourier transform (FFT) block size was 1,024 points, with the resulting frequency resolu-

tion of 68.4 Hz. Consequently, the spectra shown in this paper represent an ensemble average of 100 'instantaneous' or short-time-duration spectra with an associated random error of 10%. The uncertainty associated with the unsteady pressure  $P_{\text{rms}}$  is  $\pm 0.02$  psi.

### 3 Steady microjet actuation using POD-based control

To maintain a uniform reduction of the unsteady pressure over a wide range of operating conditions, a quasi closed-loop control method was investigated. The details of this control strategy, the analytical basis, and the results obtained are reported in this section.

#### 3.1 The proper orthogonal decomposition algorithm

As mentioned earlier, the POD method is a tool used to extract the most energetic modes from a set of realizations from an underlying system, a brief description of which is provided below. Given a flow defined on a domain  $\Omega$  over a time interval  $T$ , the flow-field variables such as velocity, pressure, and density, can be predicted using the governing equation. To ensure better accuracy, the flow is treated as a random process with parameters of time and space. We shall denote the flow variable as the sum of orthonormal basis  $a(t)$  and  $\phi(x)$ , or

$$u(x, t) = \sum_{n=1}^{\infty} a_n(t)\phi_n(x), \quad (1)$$

with the complexity of the model reduced by truncating the series at a suitable value. While a large number of basis functions  $\phi(x)$  can be used, the simplest, yet most powerful, basis function is that which is obtained using the Karhunen–Loeve expansion (1) (Newman 1996).

Using the Karhunen–Loeve expansion, the unsteady pressure is expressed as

$$p(t, \theta) = \sum_{n=1}^{\infty} \sqrt{\lambda_n} a_n(t)\phi_n(\theta) \quad (2)$$

where the temporal terms are uncorrelated and are given as

$$a_n(t) = (\sqrt{\lambda_n})^{-1} \int_{\Omega} \phi_n(\theta)p(t, \theta)d\theta \quad (3)$$



$$E[a_m(t)a_n(t)] = \delta_m^n \tag{4}$$

$$\int_{\Omega} \phi_m(\theta)\phi_n(\theta)dx = \delta_m^n \tag{5}$$

and the orthonormal basis functions  $\{ \phi_n \}$  are calculated from integral equations based on a covariance function  $R_p(\theta_1, \theta_2)$  as

$$\int_{\Omega} R_p(\theta_1, \theta_2)\phi_n(\theta_2)d\theta_2 = \lambda_n\phi_n(\theta_1), \quad \theta_1, \theta_2 \in \Omega \tag{6}$$

$$R_p(\theta_1, \theta_2) = E[(p_{\theta_1} - \mu(\theta_1))(p_{\theta_2} - \mu(\theta_2))] \tag{7}$$

where  $\mu(\theta_1), \mu(\theta_2)$  are mean values of variable  $p_{\theta_1}, p_{\theta_2}$ , respectively and  $\delta_m^n = 0$  (if  $m \neq n$ ),  $1$  (if  $m = n$ ). The derivation of the temporal term, the uncorrelated property and rigorous proofs can be found in Newman’s (1996) paper. The spatial mode  $\phi_n(\theta_1)$  can be calculated using ‘method of snap shot’ as follows (Tang et al. 2001). Let the  $p^n(j)$  be the pressure variable at a spatial point  $n$  at some time  $j$  where  $n = 1, 2, \dots, N$  and  $j = 1, 2, \dots, J$ , with  $n$  much smaller than  $J$ . Now the matrix  $Q$  can be expressed from singular value decomposition as

$$Q = \begin{pmatrix} p^1(1) & p^1(1) & \dots & p^1(J) \\ p^2(1) & p^2(1) & \dots & p^2(J) \\ p^3(1) & p^3(1) & \dots & p^3(J) \\ \vdots & \vdots & \dots & \vdots \\ p^N(1) & p^N(1) & \dots & p^N(J) \end{pmatrix} = U\Sigma V^T$$

where  $U(N \times l)$  and  $V(J \times l)$  are unitary matrix

$$[U]^T[U] = [I]_{l \times l}, \quad [V]^T[V] = [I]_{l \times l} \tag{8}$$

and

$$[\Sigma]_{l \times l} = \begin{pmatrix} \sigma_1 & & & \\ & \sigma_2 & & \\ & & \ddots & \\ & & & \sigma_l \end{pmatrix} \tag{9}$$

$\sigma_1 \geq \sigma_2 \geq \sigma_3 \geq \dots \geq \sigma_l$

The matrix  $V$  and  $\sigma$  are the Eigen vector and the square-root of the Eigen value, respectively of the correlation matrix  $Q^T Q$ .

$$[Q]^T[Q] = [V][\Sigma]^T[U]^T[U][\Sigma][V]^T = [V][\Sigma]^T[\Sigma][V]^T \tag{10}$$

The mode-shape can be computed by normalizing each column of the following matrix  $\Phi$ .

$$\Phi \equiv QV = [U][\Sigma][V]^T[V] = [U][\Sigma] = [\phi_1 \ \phi_2 \ \dots \ \phi_l]. \tag{11}$$

In short, the spatial  $i$ th POD mode can be obtained as given below:

$$\phi_i(x_n) = \sum_{j=1}^J \frac{V(j, i)Q(x_n, j)}{\sigma_i}, \quad i = 1, \dots, l; \quad n = 1, \dots, N \tag{12}$$

### 3.2 POD-based control of impingement tones

In order to find the POD modes of the system, the measurements of pressure at all flow points and a real time calculation scheme are needed. However, this is not feasible either experimentally or computationally due to obvious constraints. Fortunately, the feedback loop is most sensitive to the conditions in the immediate vicinity of the jet nozzle. Therefore we analyze the flow field by focusing only to the nozzle exit. That is, we derive the control strategy using the expansion:

$$p(\theta, t) \triangleq p_+(r = R_s, \theta, z = z_{\text{nozzle}}, t) = \sum_{i=1}^L X_i(t)\phi_i(\theta) \tag{13}$$

where  $R_s$  is the radial position of the sensors on the lift plate and  $p_+$  is the pressure outside of main jet. Note that  $\phi_i$ ’s in Eq. 13 are the spatial modes of the flow field confined to nozzle exit. Once the mode shapes are determined, we simply choose the control strategy as:

$$p_{\mu}(\theta) = k\phi_1(\theta), \tag{14}$$

where  $\phi_1$  is the most energetic mode in Eq. 13 and  $k$  is a calibration gain. The complete quasi closed-loop procedure therefore consists of collecting pressure measurements  $p(\theta, t)$ , expanding them using POD modes as in Eq. 13, determining the dominant mode  $\phi_1$ , and matching the control input—which is the microjet pressure distribution along the nozzle—to this dominant mode as in Eq. (14), and is denoted as a ‘mode-matched’ control strategy.

### 3.3 Experimental results

The mode-matched control strategy described above was implemented at the STOVl supersonic jet facility of the Fluid Mechanics Research Laboratory, FSU (Lou et al. (2002)). Four banks of microjets were distributed around the nozzle exit, while pressure

fluctuations were sensed using six *Kulite*<sup>TM</sup> transducers flush mounted around the nozzle periphery on the lift plate, at  $r/d = 1.3$ , from the nozzle centerline ( $d$  is the nozzle throat diameter).

The control experiment was performed for a range of heights (of the nozzle above ground). At each height in addition to the ‘mode-matched’ control, the open-loop control strategy described earlier where the microjet pressure around the nozzle exit was maintained at a uniform value was also implemented. To ensure a fair comparison between the two control methods, the main nozzle was operated under the same conditions while implementing these two different control strategies. The calibration constant  $k$  in Eq. 14 was chosen such that the minimum and maximum values of the POD mode over  $\theta$  correspond to 70 and 120 psia, respectively, which ensured maximum effectiveness of the actuator. The value of 70 psia was chosen since it was the lowest pressure at which any measurable control effect could be observed and 120 psia was chosen since it was the pressure that the steady control (with 20° inclination) effect is almost saturating. Figure 5a shows the shape of the first mode and the suggested microjet bank pressure distribution for several heights.

Figure 5b shows the results for the ‘‘POD-based’’ control strategy, which indicates a better performance compared to the open-loop controller throughout all operational conditions, with a large improvement at heights  $h/d = 4, 4.5,$  and  $5$ . The reason for this increased noise reduction can be attributed to the percentage of energy contained in the dominant mode, which is used in the control strategy. Seen in the Table 1, at heights 4–5, the energy content of the first mode is almost 90%. In contrast, at heights 2 and 3, the energy level drops to about 50% and hence the corresponding improvement in the closed-loop strategy also drops to about half the dB-value at heights 2 and 3 compared to at heights 4 and 5.

As noted in the introduction, flows governed by a feedback loop are highly sensitive to very small changes in the local conditions, displaying different behavior under the same nominal conditions. This is illustrated in Fig. 6, which shows the effect of control using microjets inclined at 30° with respect to the nozzle axis. A comparison of the OASPL of the uncontrolled cases in Figs. 5 and 6 shows that the noise characteristics in these two experiments are quite different, though major characteristics of the flow-field such as a monotonically decreasing OASPL as  $h/d$  increases and the overall noise level are the same. The distinct feature of this case is that the open-loop control with 30° injection led to a large amount of noise reduction without any feedback action. The POD-

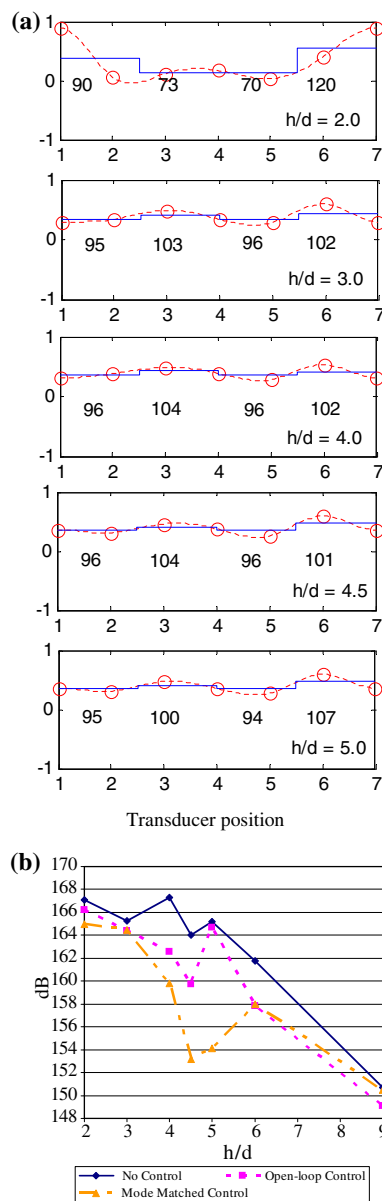


**Fig. 5** Experimental result with 20° microjet injection (Lou et al. 2002). **a** The first mode shape and suggested microjet pressure distribution for each height.  $h$  is the height of the lift plate from ground. **b** Overall sound pressure levels (OASPL) for different control (NPR = 3.7)

**Table 1** The energy content of the first four modes at each height (NPR = 3.7, 20° injection)

$h/d$	Mode1	Mode2	Mode3	Mode4
2.0	0.4615	0.2488	0.1785	0.1111
3.0	0.5515	0.2745	0.1144	0.0597
4.0	0.8609	0.0691	0.0443	0.0257
4.5	0.8836	0.0517	0.0389	0.0258
5.0	0.8736	0.0757	0.0314	0.0194

Experiment of Lou et al. (2002)

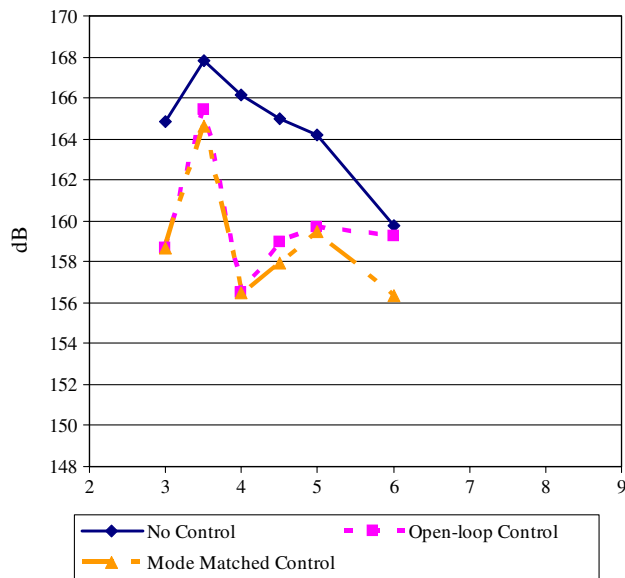


**Fig. 6** Experimental result with a 30° microjet injection. Overall sound pressure levels (OASPL) for different control (NPR = 3.7)

based control was observed to be slightly better with an additional 1–2 dB reduction over open-loop control at heights 4.5 and 6 and denoted in Fig. 6. From the energy content view (Fig. 6; Table 2), the microjet should have reduced the noise level further but the result was not as dramatic as before.

A possible reason for the occasional lack of impact from the microjets is discussed below. It has been observed in Krothapalli et al. (1999) that the flow characteristics evolve from a helical mode to an axisymmetric mode and return to a helical mode as the nozzle to ground distance becomes larger. Figure 7a shows the phase difference measured by *Kulites* mounted on the lift plate at the most dominant frequency, at  $h/d = 3.5, 4.0,$  and  $4.5$ . A small deviation in the phase difference between the signals implies that the flow characteristics are axisymmetric.

From Figs. 6 and 7a, b, we note that there is a correlation between the amount of noise reduction and the flow mode. It can be seen that at heights  $h/d = 3.5$

and 4.5, the dominant mode is helical with the helicity being stronger at  $h/d = 3.5$ , while at  $h/d = 4.0$ , the dominant mode is axisymmetric. Correspondingly, we note that the OASPL reduction is the least at  $h/d = 3.5$ , maximum at  $h/d = 4.0$ , and medium at  $h/d = 4.5$ . That is, the lack of noise reduction appears to be correlated with the presence of a helical mode in the 30°-injection case. This is also consistent with the results of the 20°-injection case reported in Fig. 5, where the dominant mode was predominantly axisymmetric at most heights. A low OASPL reduction of 1 dB occurring at  $h/d = 3.0$  for the 20°-injection case could therefore be due to the fact that the component of the axisymmetric mode at this height was 55%, which was less than the amount of axisymmetric mode present at other  $h/d$ . One could argue that the specific case of  $h/d = 4.5$  with 30°-injection shown in Fig. 6 is somewhat of an exception to the above hypothesis, which links lack of reduction to the presence of a helical mode. At this  $h/d$ , an OASPL reduction of 7 dB occurs despite the presence of a helical mode. This anomalous behavior could be due to the fact that the helical effect at the nozzle becomes less important as  $h/d$  increases.

A final observation is a comparison between the amount of noise reduction achieved in Figs. 5 and 6, which corresponds to a microjet injection of 20° and 30°, respectively. We note that larger reductions occur in the latter case, which is most likely due to the fact that with a larger injection angle, a greater penetration depth of the microjet streak into the shear-layer of the primary jet is achieved, as shown in Lou (2005). At a given angle of injection, a larger penetration depth is always achievable by raising the mass-flux. However, increasing the mass-flux may not often be desirable due to practical constraints. Therefore, any actuation method that leads to a larger penetration depth at reduced mass-flux rates has a good chance of assuring a larger and more consistent noise reduction at all operating conditions. In the next section, we present the results of a different actuation method that has the above desirable property.

#### 4 Pulsed microjet actuation using a rotating cap

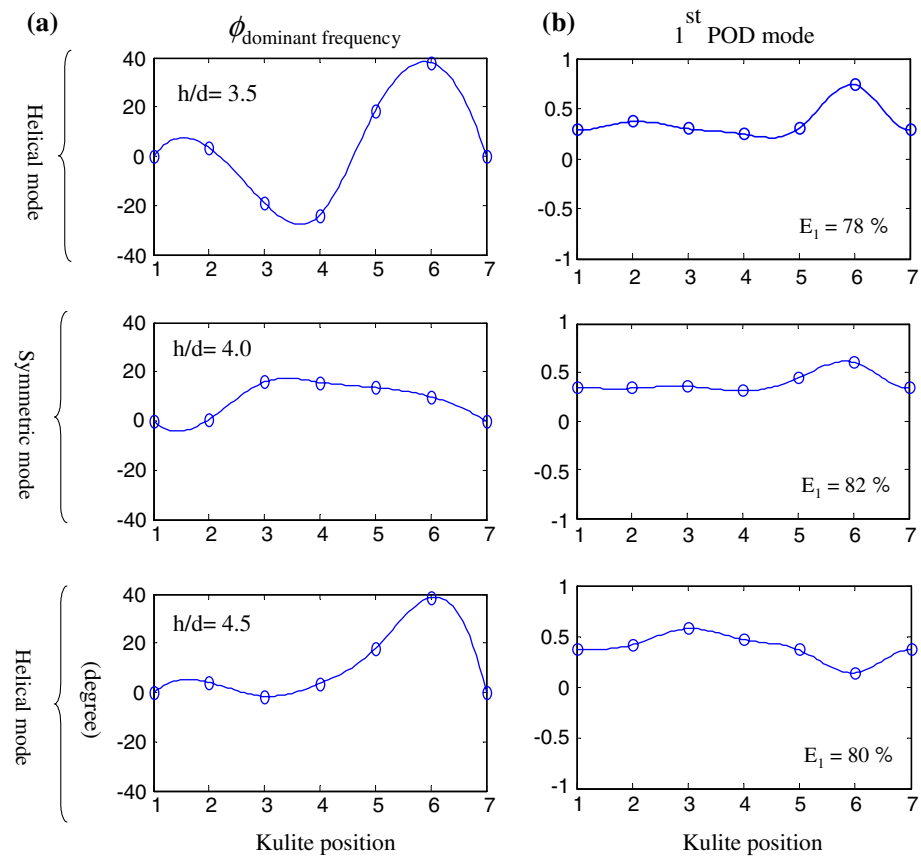
The results in Sect. 3 show that a ‘quasi-closed loop control’ method produced additional noise reduction compared to the open-loop control strategy. To obtain a more consistent noise reduction over a larger range of jet operating conditions, we examined a different control strategy, which consists of a technique that *pulses* the microjet flow. The rationale for introducing pulsing is discussed below.

**Table 2** The energy content of the first four modes at each height (NPR = 3.7, 30° injection)

h/d	Mode1	Mode2	Mode3	Mode4
3.0	0.5796	0.1750	0.1359	0.1095
3.5	0.7800	0.1526	0.0371	0.0303
4.0	0.8262	0.0700	0.0563	0.0475
4.5	0.8060	0.1005	0.0679	0.0257
5.0	0.8114	0.1038	0.0552	0.0297
6.0	0.8096	0.0938	0.0506	0.0461



**Fig. 7** Experimental result with a 30° microjet injection. **a** Phase difference between the six Kulites corresponding to the dominant frequency. **b** The first POD mode for corresponding heights without control.  $E_1$ : the energy content of the first POD mode



For a given mass flow rate  $\dot{m} = \rho A U_{\mu,0}$ , the force induced by steady microjet injection is given by the rate of momentum change in time. Using the same mass flow rate, an unsteady injection can exert more force on the primary jet shear layer of the flow than steady injection, in an average sense. Equation 15 described below shows that, if as an example, the unsteady flow through the microjets is represented in sinusoidal form, the additional force increase is realized by  $\rho A (B^2/2)$ :

$$\begin{aligned}
 F_{\mu,\text{steady}} &= \dot{m}U_{\mu,0} = \rho A U_{\mu,0}^2 \\
 U_{\mu,\text{unsteady}} &= U_{\mu,0} + B \sin(\omega t) \\
 F_{\mu}(t) &= \dot{m}U_{\mu,\text{unsteady}} = \rho A (U_{\mu,0} + B \sin(\omega t))^2 \\
 \overline{F_{\mu}(t)} &= \frac{\omega}{2\pi} \int_0^{2\pi/\omega} \dot{m}U_{\mu,\text{unsteady}} dt \\
 &= \rho A \left( U_{\mu,0}^2 + \frac{B^2}{2} \right) \tag{15}
 \end{aligned}$$

That is, for a given mass flow rate, a pulsed injection can generate more momentum than steady continuous microjet injection, and hence can perhaps have a stronger impact on the jet shear layer, thus disrupting

the feedback mechanism more effectively and hence reducing the noise more significantly.

#### 4.1 Pulsing using a rotating cap

Flow modulation was introduced using direct modulation at the exit of the microjet using a rotating cap (Fig. 8). This cap consists of several teeth which block and unblock the microjet holes as the cap rotates, simulating an on-off microjet action. The design of the lift plate is slightly changed to install the rotating cap actuator, and is composed of a small and a large lift plate (Figs. 9, 10). The small lift plate is assembled along with the rotating cap at the center of the big lift plate using a bearing. A motor mounted behind the lift plate drives the rotating cap connected by a belt. Finally, the lift plate is supported by three arms attached to the holder which itself is attached to a pipe supplying air to the main nozzle. Figure 11 shows the lift plate assembly.

The effect of the pulsed microjets through the rotating cap was quantified by spinning the motor at different speeds and measuring the unsteady total pressure at the microjet exit using a *Kulite* mounted in a total pressure probe configuration. These measure-

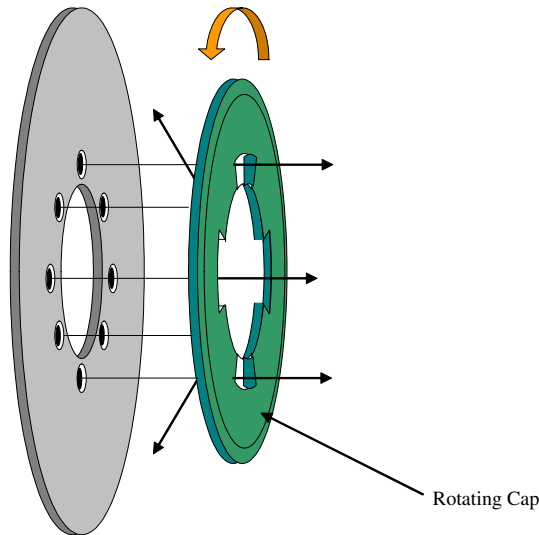


**Fig. 8** Conceptual diagram for rotating cap actuator

ments were sampled at 70 kHz with a cut-off frequency of 33 kHz. In Fig. 12a, b, the pressure response with respect to time using a steady and pulsed microjet flow are shown, respectively. In Fig. 12c, the power spectra corresponding to the time series in Fig. 12b shows that

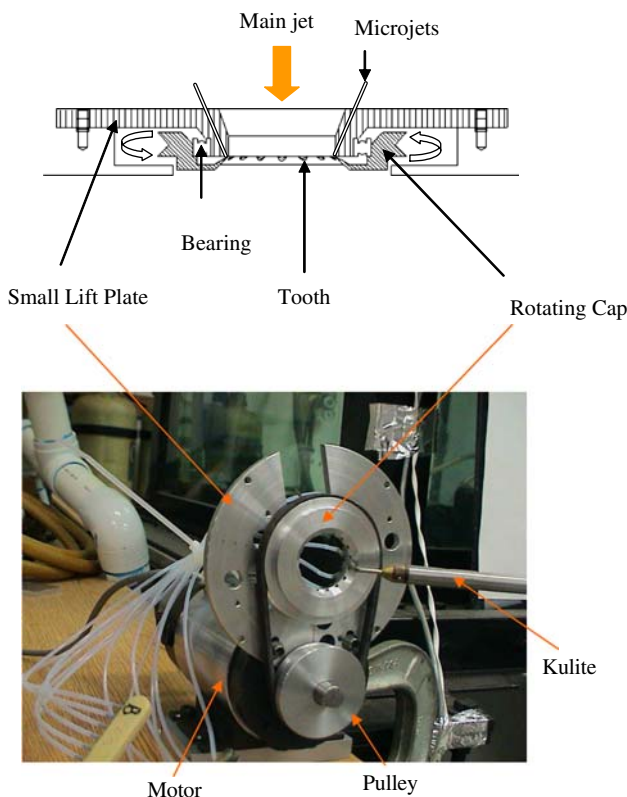


**Fig. 9** Rotating cap design

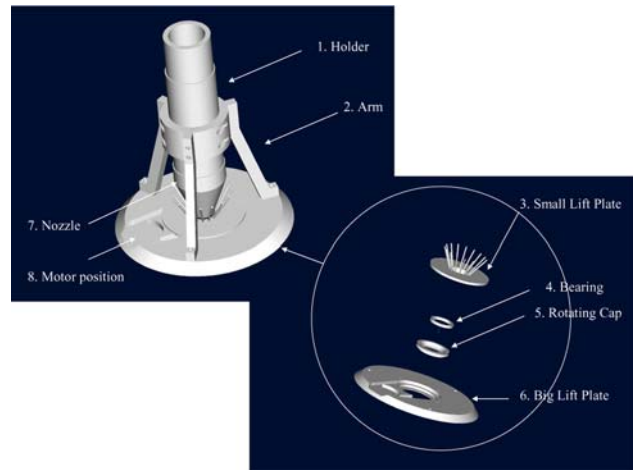


**Fig. 10** Assembled feature of lift plate and nozzle

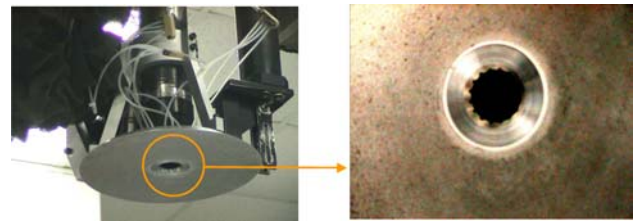


**Fig. 11** Experimental setup installed with lift plate

the rotating cap produces a fairly large amplitude perturbations around 300 Hz. This unsteady effect was observed for motor speeds over a range of 0–2,000 rpm. The speed of pulsing is determined by the motor speed, the diameter of rotating cap and number of teeth in the cap. One revolution of the cap introduces 16 pulses since the cap has 16 internal holes. Moreover, the pulley which drives the rotating cap has a smaller diameter than the rotating cap. Hence, the pulsing speed is obtained from the following relations:

$$f_{\text{pulsing}} = 16 \times (D_{\text{pulley}}/D_{\text{cap}})RPM_{\text{pulley}}/(60) \quad (16)$$

where  $D_{\text{cap}} = 2.625$  in.,  $D_{\text{pulley}} = 2$  in. Here the resultant pulsing speed by the rotating cap was set to 121 Hz, which corresponds to a moderate motor speed of 596 rpm. At this speed, the vibrations due to the rotating mechanism are minimal and do not lead to a broadband noise increase.

In addition to providing a direct method of pulsing the microjet flow, it is also of interest to be able to vary different parameters of the pulsed flow such as amplitude, frequency, duty-cycle, and phase. This can be accomplished by varying the design parameters of the rotating cap. The pulsing amplitude is directly

proportional to the supply pressure delivered to microjet chamber, while pulsing frequency is solely controlled by the rotation speed of the cap. Therefore, these two parameters can be easily and electronically varied by changing the microjet pressure and the motor speed. The duty cycle and the phase, on the other hand, depends on the design of the rotating cap and requires a mechanical design procedure. For example, if  $d_c$  is the duty cycle of pulsing, which is the ratio of the valve opening time to pulsing period, then

$$d_c = 100 \left( \frac{N_h d_h}{\pi d} \right) \% \tag{17}$$

where  $d$  is the main jet diameter,  $d_h$  is the diameter of the holes in the rotating cap (Fig. 13), and  $N_h$  is the number of holes in the rotating cap. This implies that the duty cycle ( $d_c$ ) is changed by varying the number and diameter of the holes of the rotating cap. If the number of holes in the rotating cap is the same as that of microjets, all the microjets pulse synchronously. To achieve a phase difference between two adjacent microjet pulses, the number of holes in the cap was chosen to be different from that of microjets. This phase difference,  $\phi_{\text{phase}}$ , can be calculated using Eq. 18

$$\phi_{\text{phase}} = \left( \frac{N_h}{N_m} - 1 \right) \times 360 \tag{18}$$

where  $N_m$  is the number of microjets.

We illustrate a realization of  $\phi_{\text{phase}} = 120^\circ$  in Fig. 14, which occurs by choosing  $N_h = 4$  and  $N_m = 3$ . This configuration produces pulsing with  $\phi_{\text{phase}} = 120^\circ$ . In the impinging jet problem, 18 ( $N_h$ ) holes were made in the rotating cap while 16 ( $N_m$ ) microjets were installed in the lift plate. From Eq. (18), we observe that this produces a  $\phi_{\text{phase}}$  of  $45^\circ$ .

It should be pointed out that the swirl caused by the cap rotation itself does not significantly affect the baseline performance. This is demonstrated in Fig. 15, where the OASPL of the uncontrolled impinging jet is compared to that while the cap was rotating without any microjet action. As can be seen in the figure, the two OASPLs are almost identical.

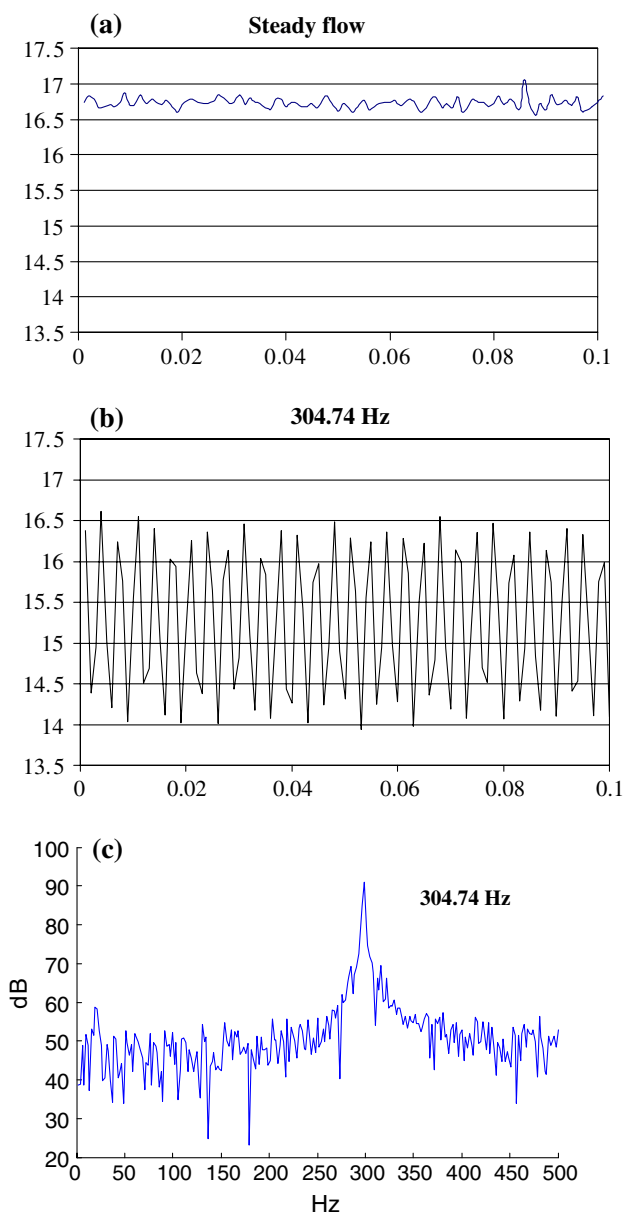


**Fig. 12** Performance of collocated rotating cap actuator; total pressure data in time series. **a** Case of steadily injecting microjet. **b** Case of pulsing microjet at the speed of 304.74 Hz. **c** Power spectra plot of pulsing microjet

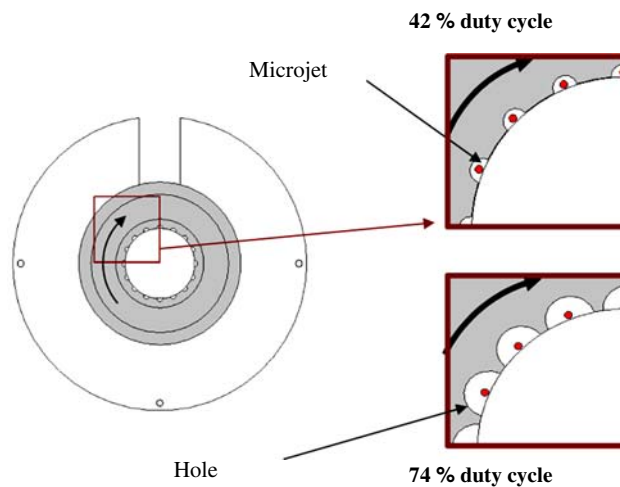
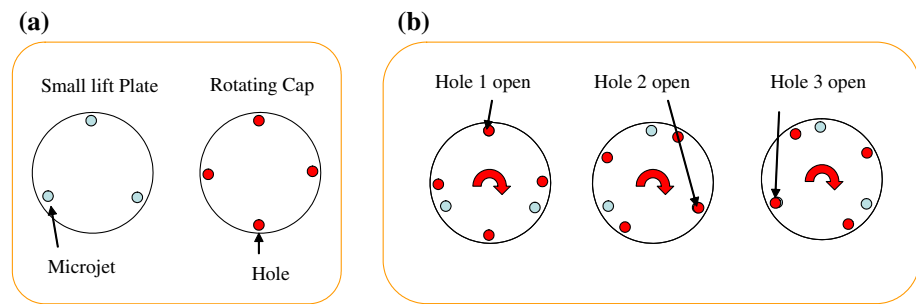


**Fig. 13** Modification of duty cycle by changing hole size

**Fig. 14** Concept of pulsing with phase difference. **a** Configuration of lift plate and rotating cap. **b** Microjet pulsing in the consecutive stages



As mentioned in Sect. 1, a similar design to the rotating cap approach discussed above has been reported in Ibrahim et al. (2002) for suppressing jet noise. A comparison between our design and that of Ibrahim et al. (2002) is briefly illustrated in Fig. 16. The major distinction between the two is the distance from the microjet injection point to the shear layer of main jet. In Ibrahim et al. (2002) shown in Fig. 16a, 36 microjets with a diameter of 0.5 mm were used, with a mass flow rate of 2–4% that of primary jet. But the location of the microjets were at five-diameters away from the shear-layer of the main jet on the azimuthal plane. Our design, shown in Fig. 16b, collocates the actuator with the nozzle exit, thereby allowing the microjet flow to have an inclination angle with respect to the flow direction. In contrast, in Ibrahim et al. (2002), the microjet injection is forced to remain normal to the main flow. The lack of success reported in Ibrahim et al. (2002) may in part be due to the location of the actuators, since the penetration depth of microjet injection into the shear layer is known to play a critical role in the noise suppressing mechanism.

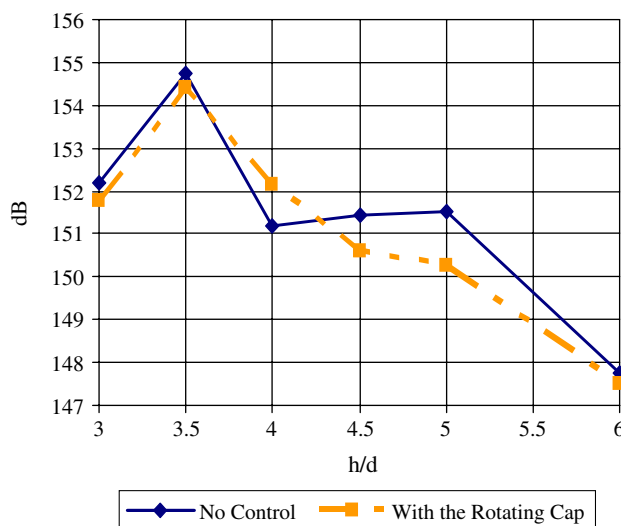


**Fig. 15** OASPL with cap rotating

## 4.2 Results using pulsed microjets

Using the above experimental setup, studies of the impinging jets were conducted with and without pulsing. Unlike ‘POD-based control’ case, the unsteady pressure measurements could not be obtained on the lift plate due to the vibrations from the spinning cap incorporated in the small lift plate (Figs. 8, 10). Instead the noise level was measured by a microphone located at 25 cm away from the nozzle axis. The results obtained when the rotating cap was spun at a frequency of  $f = 121$  Hz and  $\phi_{\text{phase}} = 0$ , and  $d_c = 74\%$  are shown in Fig. 17b. These results show that the impinging tones are completely eliminated by the pulsed microjets. In order to further understand the impact of the rotating cap and the sensitivity of the impinging flow field to the pulsing parameters such as frequency and duty-cycle, a number of parametric studies were conducted, which are summarized below:

**(a) Effect of duty-cycle ( $d_c$ )** The effect of duty-cycle was explored and is presented in Fig. 17a, b. These were obtained for two different duty-cycles of 42 and 74% at a pulsing frequency of 121 Hz with 115 psia microjet supply pressure. Two points should be noted from this figure. The first is that both pulsing and steady microjet action yield about the same amount of pressure reduction, and since the supply pressures were

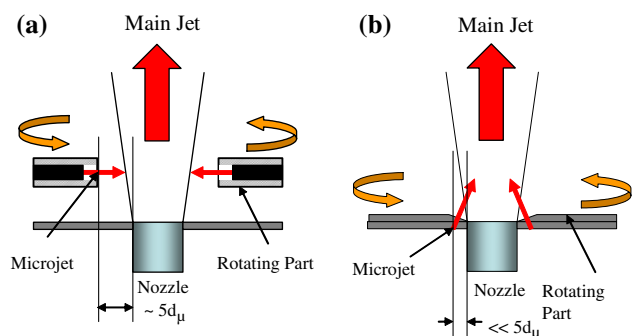
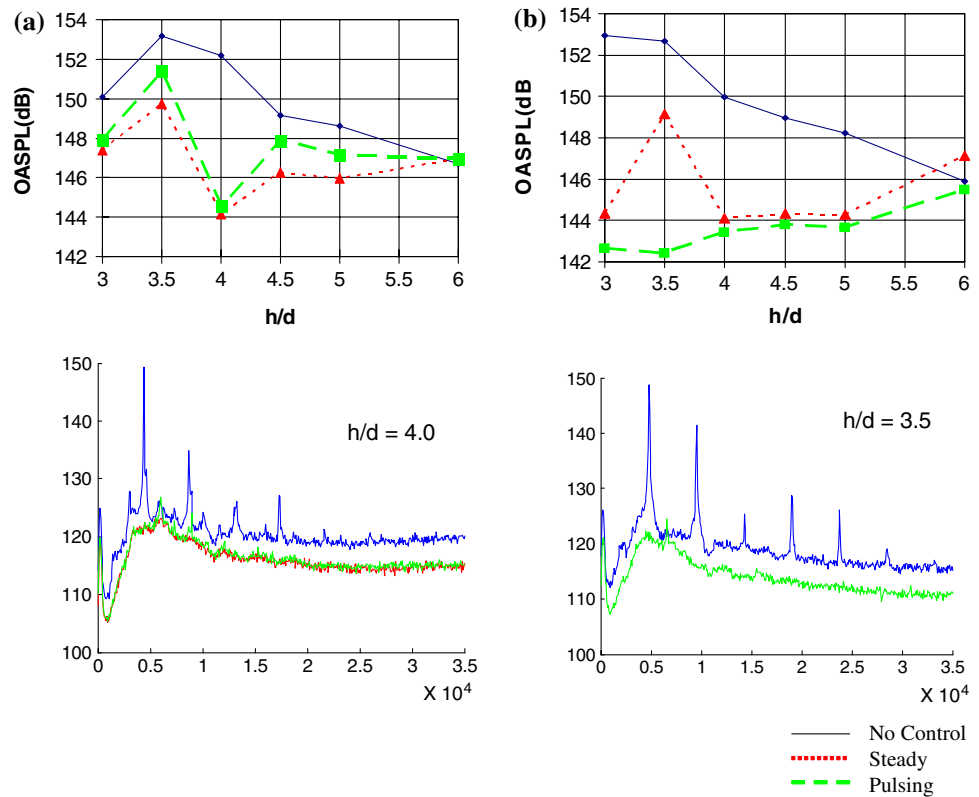


**Fig. 16** **a** Rotating cap design in reference (Ibrahim et al. 2002). **b** Collocated rotating cap used in this paper

**Fig. 17** Experimental result using synchronous pulsing scheme. **a** Case of  $d_c = 42\%$ . **b** Case of  $d_c = 74\%$



the same, it implies that the pulsing action allows noise reduction to occur at 42% of the mass flow rate needed for the steady case. The second is that a significantly larger reduction can be obtained from the pulsing action under certain duty cycles, which follows from Fig. 17b. It was in fact observed that the pulsed injection completely destroyed the distinct impinging tones at almost all  $h/d$ . Moreover, this occurred at a mass flow rate that is 74% of the steady injection case. Yet another point to note is the robustness of the pulsed actuation method. It should be noted that the amount of noise in the no-control case is a little different in the two different experiments shown in Fig. 17a, b—primarily at  $h/d = 3$  and 4—due to the sensitivity of impinging jet properties on slight changes in the boundary conditions. Nevertheless, the lack of reduction using steady microjet injection at the height  $h/d = 3.5$  is consistent between the two experiments. In contrast in both cases, the pulsed injection maintains to an additional reduction of 2 dB or more at this height.

**(b) Effect of frequency ( $f_{pulsing}$ )** The rotating cap was spun over a range of frequencies from 0 to 150 Hz, corresponding results of which are shown in Fig. 18. This shows that over this range, the amount of noise reduction is quite independent of  $f_{pulsing}$ . To prevent the possible damage from friction of rotating part and

make the whole assembly working safe, we chose the pulsing frequency  $f_{pulsing}$  as 121 Hz as the primary test case.

**(c) Effect of phase-difference  $\phi_{phase}$**  As mentioned in Sect. 3.3 and illustrated in Fig. 7, we initially anticipated that the phase difference will play an important role in noise reduction mechanism. Two experiments were conducted by changing the rotating direction of

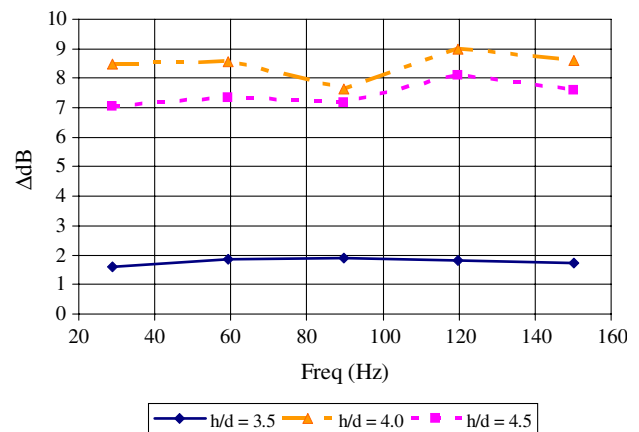
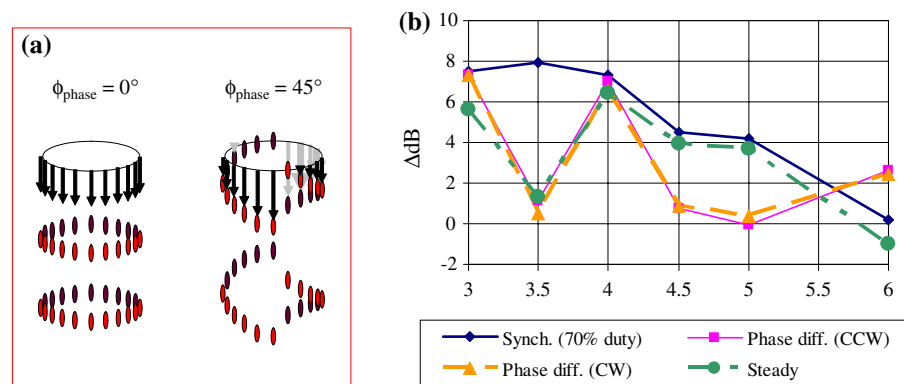


**Fig. 18** Noise reduction for different pulsing frequencies,  $d_c = 42\%$  (x-axis represents pulsing frequency, y-axis denotes noise reduction in dB scale)



**Fig. 19** **a** Flow of pulsing with different phase. **b** Implementation of pulsing with phase difference. Supply pressure to microjet: 115 psia



the cap to check the effect of phase lead and phase lag on noise reduction. The duty cycle was set at 50%, the supply pressure delivered to the microjet chamber was set to 115 psia, and the pulsing speed was 121 Hz. The results obtained for a phase of  $45^\circ$  and  $-45^\circ$  are shown in Fig. 19 and compared with the synchronously pulsed injection case, where the duty cycle was maintained at 42%. We note that these phase variations did not result in any noticeable improvement over the synchronous scheme and uneven noise reduction for various heights is still conspicuous. While the reason for this remains unresolved, more experiments are being planned to understand the role of phase difference in pulsed microjet actuation.

## 5 Summary

In this paper, active control of supersonic impinging jets using microjets is considered. A ‘quasi-closed loop control’ is derived in this paper based on the POD method which determines the most energetic mode at the nozzle exit along the azimuthal direction is used as the control input. By matching the intensity of microjets’ supply pressure to this mode, we could achieve an additional 8–10 dB reduction compared to an open loop. This quasi closed-loop strategy, called ‘mode-matched control,’ demonstrated a significant noise reduction, but its amount was found to be nonuniform and vary with operating conditions. Hence, a pulsing microjet was introduced as a new actuator because the unsteadiness of the microjet flow can increase the forcing strength and thus have a more significant impact on the shear layer of the main jet. The pulsing was accomplished by way of a saw-toothed rotating cap that was incorporated in the lift plate and spinning it so that the saw-tooth periodically blocks and unblocks the microjet flow. Using this method, we were able to pulse the microjet flow up to

several hundred hertz. But this pulsing speed is still far below than the natural frequency of the impinging tone ( $\sim 5$  kHz).

Several parameters of the pulsing were varied to determine conditions under which the flow structure and noise reduction were most receptive to. It was observed that variations in the duty-cycle of the pulsing led to a maximum impact. A pulsed microjet with a duty cycle of about 40% achieved the same amount of reduction as a steady microjet with comparable plenum pressure. A pulsed microjet with a duty cycle of about 75% led to a much higher overall reduction, and completely destroyed the distinct impinging tones at almost all heights. Changing the phase difference of the pulsing was also found to reduce the impinging tones, albeit to a smaller extent compared to the duty cycle. Currently, work is on-going to determine the optimal values for the frequency, duty-cycle, and phase of pulsing that lead to consistent and large reduction as operating conditions vary.

**Acknowledgments** This work was supported by a grant from AFOSR, monitored by Dr. J. Schmisser. We would like to thank the staff of FMRL, for their invaluable help in conducting these tests. We are grateful to Mr. Choutapalli for his help in conducting the tests, and Robert Avant for his advice in designing the experimental setup. In addition, Mr. DePriest’s prompt support made it possible to implement several crucial tests.

## References

- Alvi FS, Shih C, Elavarasan R, Garg G, Krothapalli A (2003) Control of supersonic impinging jet flows using supersonic microjet. *AIAA J* 41(7):1347–1355
- Annaswamy AM, Fleifil M, Rumsey JW, Prasanth R, Hathout JP, Ghoniem AF (2000) Thermoacoustic instability: model-based optimal control designs and experimental validation. *IEEE Trans Control Syst Technol* 8(6):905–918
- Arndt REA, Long DF, Glauser MN (1997) The proper orthogonal decomposition of pressure fluctuations surrounding a turbulent jet. *J Fluid Mech* 340:1–33

- Bakewell P, Lumley JL (1967) Viscous sublayer and adjacent wall region in turbulent pipe flow. *Phys Fluids* 10:1880–1889
- Cattafesta L, Alvi F, Williams D, Rowley C (2003) Review of active control of flow-induced cavity oscillations. Technical Report 2003-3567, AIAA Paper
- Cipolla KM, Liakopoulos A, Rockwell DO (1998) Quantitative imaging in proper orthogonal decomposition of flow past a delta wing. *AIAA J* 36(7):1247–1255
- Citriniti JH, George WK (2000) Reconstruction of the global velocity field in the axisymmetric mixing layer utilizing the proper orthogonal decomposition. *J Fluid Mech* 418:137–166
- Delville J, Ukeiley L, Cordier L, Bonnet JP, Glauser M (1999) Examination of large-scale structures in a turbulent plane mixing layer. Part 1. Proper orthogonal decomposition. *J Fluid Mech* 391:91–122
- Elavarasan R, Krothapalli A, Venkatakrishnan L, Lourenco L (2002) Suppression of self-sustained oscillations in a supersonic impinging jet. *AIAA J* 39(12):2366–2373
- Erengil ME, Dolling DS (1993) Effects of sweepback on unsteady separation in mach 5 compression ramp interactions. *AIAA J* 31(2):302–311
- Glass D (1968) Effect of acoustic feedback on the spread and decay of supersonic jets. *AIAA J* 6(10):1890–1897
- Holmes P, Lumley JL, Berkooz G (1996) Turbulence, coherent structures, dynamical systems and symmetry. Cambridge University Press
- Ibrahim MK, Kunimura R, Nakamura Y (2002) Mixing enhancement of compressible jets by using unsteady microjets as actuators. *AIAA J* 40(4):681–688
- Kastner J, Samimy M (2003) Effects of forcing frequency on the control of an impinging high-speed jet. Technical Report 2003-0006, AIAA Paper
- Krothapalli A, Rajakuperan E, Alvi FS, Lourenco L (1999) Flow field and noise characteristics of a supersonic impinging jet. *J Fluid Mech* 392:155–181
- Lou H (2005) Control of supersonic impinging jets using microjets. Ph.D. Thesis, Florida State University
- Lou H, Alvi FS, Shih C, Choi J, Annaswamy AM (2002) Flow-field properties of supersonic impinging jets with active control. Technical Report 2002-2728, AIAA Paper
- Ma X, Karamanos GS, Karniadakis G (2000) Dynamics and low-dimensionality of a turbulent near wake. *J Fluid Mech* 410:29–65
- Newman A (1996) Model reduction via the karhunen-loève expansion. technical research report, t. r. Technical Report 96-32, 96-33, Institute for Systems Research, University of Maryland, Maryland, USA
- Poldervaart LJ, Wijnands APJ, van Moll L H A M, van Voorhuizen EJ (1974) Modes of vibration. Audio-visual Cent. Eindhoven Univ. Tech., The Netherlands
- Raman G, Kibens V (2001) Active flow control using integrated powered resonance tube actuators. Technical Report 2001-3024, AIAA Paper
- Rempfe D (1994) On the structure of dynamical systems describing the evolution of coherent structures in a convective boundary layer. *Phys Fluids* 6:1402–1404
- Rowley CW, Colonius T, Murray RM (2000) Pod based models of self-sustained oscillations in the flow past an open cavity. Technical Report 2000-1969, AIAA Paper
- Sheplak M, Spina EF (1994) Control of high-speed impinging-jet resonance. *AIAA J* 32(8):1583–1588
- Shih C, Alvi FS, Washington D (1999) Effects of counterflow on the aeroacoustic properties of a supersonic jet. *J Aircr* 36(2):451–457
- Sinha N, Arunajatesan S, Seiner JM (2002) Computational and experimental investigations of cavity attenuation using high frequency control. Technical Report 2002-2403, AIAA Paper
- Sirovich L, Rodriguez JD (1987) Coherent structures and chaos: a model problem. *Phys Lett A* 120(5):211–214
- Stanek MJ, Raman G, Ross JA, Odedra J, Peto J, Alvi FS, Kibens V (2002a) High frequency acoustic suppression—the role of mass flow & the notion of superposition. Technical Report 2002-2404, AIAA Paper
- Stanek MJ, Sinha N, Seiner JM, Pearce B, Jones MT (2002b) Applying very high frequency excitation to the problem of tactical directed energy beam propagation. Technical Report 2002-2272, AIAA Paper
- Tang D, Kholodar D, Juang J, Dowell EH (2001) System identification and proper orthogonal decomposition method applied to unsteady aerodynamics. *AIAA J* 39(8):1569–1576
- Ukeiley LS, Murray N (2005) Velocity and surface pressure measurements in an open cavity. *Exp Fluids* 38:656–671
- Unalms O, Clemens N, Dolling D (2001) Experimental study of shear-layer/acoustics coupling in mach 5 cavity flow. *AIAA J* 39(2):242–252
- Wiltse JM, Glezer A (1998) Direct excitation of small-scale motions in free shear flows. *Phys Fluids* 10:2026–2036